Journal of Rock Mechanics and Geotechnical Engineering 16 (2024) 2326–2340

Contents lists available at ScienceDirect

Journal of Rock Mechanics and Geotechnical Engineering

journal homepage: www.jrmge.cn

Full Length Article

Semi-analytical solution for drained expansion analysis of a hollow cylinder of critical state soils

He Yang [a,b], Jialiang Zhang [a], Haisui Yu [b], Peizhi Zhuang [a,*]

[a] School of Qilu Transportation, Shandong University, Jinan, 250002, China
[b] School of Civil Engineering, University of Leeds, Leeds, LS2 9JT, UK

ARTICLE INFO

Article history:
Received 17 April 2023
Received in revised form
20 September 2023
Accepted 19 October 2023
Available online 28 January 2024

Keywords:
Cavity expansion
Drained analysis
Boundary effect
Critical state soil
Non-self-similar
Eulerian-Lagrangian approach

ABSTRACT

The expansion of a thick-walled hollow cylinder in soil is of non-self-similar nature that the stress/deformation paths are not the same for different soil material points. As a result, this problem cannot be solved by the common self-similar-based similarity techniques. This paper proposes a novel, exact solution for rigorous drained expansion analysis of a hollow cylinder of critical state soils. Considering stress-dependent elastic moduli of soils, new analytical stress and displacement solutions for the non-self-similar problem are developed taking the small strain assumption in the elastic zone. In the plastic zone, the cavity expansion response is formulated into a set of first-order partial differential equations (PDEs) with the combination use of Eulerian and Lagrangian descriptions, and a novel solution algorithm is developed to efficiently solve this complex boundary value problem. The solution is presented in a general form and thus can be useful for a wide range of soils. With the new solution, the non-self-similar nature induced by the finite outer boundary is clearly demonstrated and highlighted, which is found to be greatly different to the behaviour of cavity expansion in infinite soil mass. The present solution may serve as a benchmark for verifying the performance of advanced numerical techniques with critical state soil models and be used to capture the finite boundary effect for pressuremeter tests in small-sized calibration chambers.

1. Introduction

Cavity expansion theory is concerned with the changes in stresses and displacements caused by the expansion of a cylindrical/spherical cavity (Yu, 2000). This theory has been proved to be a versatile and useful tool for the interpretation of pressuremeter tests and cone penetration tests (Gibson and Anderson, 1961; Hughes et al., 1977; Chang et al., 2001; Ghafghazi and Shuttle, 2008; Mo et al., 2020), bearing capacity estimation of piles and anchors (Vesic, 1972; Randolph et al., 1994; Zhuang and Yu, 2018, Zhuang et al., 2021b), prediction of tunnel stability and deformation (Mair and Taylor, 1993; Yu and Rowe, 1999; Zhuang et al., 2022). The majority of previous studies focused mainly on cavities embedded in an infinite soil mass, which might be suitable for the analyses of many in situ geotechnical engineering problems. However, significant outer boundary effect may exist in some geotechnical problems, such as pressuremeter tests and cone penetration tests in small-sized calibration chambers (Jewell et al., 1980; Fahey, 1986; Schnaid and Houlsby, 1991; Salgado et al., 1997; Zhuang et al., 2021a; Song et al., 2022; Li et al., 2023). Due to the outer boundary effect, soil material points at different radial locations do not share the same stress/deformation path, which means that the cavity expansion process becomes non-self-similar (i.e. different stress/deformation path).

Quasi-static cavity expansion is a typical boundary value problem that can generally be expressed into a set of governing equations such as stress equilibrium equations, displacement compatibility conditions, and stress-strain relationships. Over the past decades, numerous solutions for solving this problem have been developed (Yu, 2000), among which the analytical/semi-analytical approaches can be broadly categorised into two groups (Yu and Carter, 2002), namely the auxiliary variable approach and the total strain approach.

The auxiliary variable approach was first used by Hill (1950) (also known as Hill's incremental velocity method or similarity

* Corresponding author.
E-mail address: zhuangpeizhi@sdu.edu.cn (P. Zhuang).
Peer review under responsibility of Institute of Rock and Soil Mechanics, Chinese Academy of Sciences.

https://doi.org/10.1016/j.jrmge.2023.10.018

technique) for the cavity expansion analysis in Tresca materials, in which the radius of the elastic-plastic interface is taken as the timescale. Hill's approach was then followed for the analyses of cavity expansion problems in dilatant cohesive-frictional Mohr-Coulomb soils (Yu and Carter, 2002; Carter and Yu, 2022) and critical state soils (Collins et al., 1992; Zhou et al., 2021). Another branch of this approach transforms the governing partial differential equations (PDEs) in terms of material time and spatial derivatives (i.e. Lagrangian and Eulerian descriptions, respectively) into ordinary differential equations (ODEs) by auxiliary variables (Chen and Abousleiman, 2013; Su, 2021). Taking more advanced soil models, this powerful approach has recently been used to investigate the effects of factors such as stress and material anisotropy, soil structure, unsaturated state, and temperature on the cavity expansion behaviour (Russell and Khalili, 2006; Li et al., 2016, 2021a, 2021b; Zhou et al., 2018; Chen and Liu, 2019; Chen et al., 2020; Yang et al., 2021; Chen and Mo, 2022; Mo et al., 2022). Nevertheless, it needs to be highlighted that this approach was developed on the basis of self-similarity of stress and strain configurations (i.e. every material point shares the same stress/deformation path) (Hill, 1950; Collins et al., 1992; Yu and Carter, 2002; Chen and Abousleiman, 2013; Yang et al., 2023). As such, this approach is generally appropriate for the expansion of a cylindrical/spherical cavity in an infinite soil mass, but not for cavity expansion in the non-self-similar process (e.g. in a bounded soil mass under drained conditions).

In the total strain approach, the incremental form of constitutive equations is integrated directly to result in a relationship between effective stresses and total strains. Then the time integral of deformation rates can be expressed by logarithmic strains (Chadwick, 1959), which enables Eulerian stresses/strains at an instant of time to be related to the motion of each soil material point. This approach has been successfully applied to the analyses of cavity expansion problems in various perfectly elastic-plastic materials (Gibson and Anderson, 1961; Bigoni and Laudiero, 1989; Yu and Houlsby, 1991). When more sophisticated soil models (e.g. critical state models) are employed, analytical or semi-analytical solutions may also be obtained with this approach for undrained cavity expansion analyses due mainly to the constant-volume simplification (Collins and Yu, 1996; Cao et al., 2001; Silvestri and Abou-Samra, 2012; Vrakas, 2016; Wang and Chen, 2022), whereas solutions for drained analyses were rarely reported with the approach. In addition, it needs to be mentioned that the total strain method suits the analyses of both self-similar (e.g. cavity expansion in infinite soils) and non-self-similar cavity expansion problems (e.g. a pressurised cavity in soil mass of a finite radial extent) (Yu, 1992; Zhuang et al., 2021a).

There are only a few solutions for cavity expansion in a bounded soil mass to account for the boundary effects. For example: (i) Using the total strain approach, Yu (1992, 1993) derived large strain solutions for the drained analysis of a pressurised hollow cylinder and sphere, respectively, adopting the elastic-perfectly plastic Mohr-Coulomb model. Zhuang et al. (2021a) proposed a general solution procedure for the expansion/contraction analysis of a hollow cylinder/sphere of Cam Clay soils under undrained conditions, but the approach can hardly be adopted for analyses under drained conditions because the analytical form of stress-total strain relationship is difficult to be obtained; and (ii) For cavity expansion analysis in bounded critical state soils under drained conditions, only a few approximate solutions have been developed using the self-similar-based auxiliary variable approach and assuming the radius of the elastic-plastic boundary is always smaller than the outer radius of the soil mass (Pournaghiazar et al., 2013; Cheng et al., 2018; Cheng and Yang, 2019). Consequently, rigorous drained analysis of boundary effects in the common cavity expansion problem with advanced soil models highly relies on cumbersome numerical methods (Osinov and Cudmani, 2001).

According to the above analyses, it can be concluded that neither the total strain approach nor the auxiliary variable approach can be directly applied to the drained cavity expansion in a finite critical state (Cam Clay) soil mass. While rigorous analyses for this kind of problem can depend on numerical methods such as the finite element method (FEM), analytical/semi-analytical cavity expansion solutions are equally important as they can: (i) provide an alternative tool for validating the advanced numerical techniques and (ii) be more accessible to a wide range of users to incorporate complex constitutive models. To fill the gap, this paper develops a rigorous semi-analytical method for the drained expansion analysis of a hollow cylinder of critical state soils. The considered problem is defined at first, which is followed by developing the novel solution method and calculation algorithm. The proposed method is validated by comparing with FEM and other published solutions in special cases, and its relationships with the auxiliary variable approach and total strain approach are discussed. Then a thorough parametric analysis is conducted to investigate the non-self-similar behaviour of cavity expansion in a bounded soil mass. Finally, conclusions are drawn in the last part of this paper.

2. Problem definition and assumptions

As depicted in Fig. 1a, a hollow cylinder of soil with an infinite length is considered, which is initially subjected to horizontal stress σ_{h} and vertical stress σ_{v}. The initial inner and outer radii of the cylinder are a_0 and b_0, respectively. Then the cylinder is internally pressurised with a sufficiently slow speed under perfectly drained conditions, and the expansion analysis is conducted under plane strain conditions with respect to the vertical direction. As the pressure at the inner wall increases from σ_{h} to the current inner pressure σ_a, the inner and outer radii of the soil cylinder become a and b, respectively, and the vertical stress changes to be σ_z. The soil is assumed to be isotropic and homogenous, which is modelled by the Cam-Clay-type critical state models. Once yielding occurs, a plastic zone with an outer radius of ρ may appear as shown in Fig. 1b. In the concerned plane, a cylindrical coordinate system (r, θ, z) with the origin located at the cavity centre is used for the sake of convenience.

As drained conditions are assumed, all stresses will be taken as the effective stresses by default in this study. As defined in Fig. 1, the stress boundary conditions of the problem can be expressed as

$$\sigma_r|_{r=a} = \sigma_a \tag{1}$$

$$\sigma_r|_{r=b} = \sigma_{\mathrm{h}} \tag{2}$$

where σ_r is the radial stress, and r is the current radial position of a soil material point.

The body forces are neglected in the typical quasi-static cavity expansion analysis (Yu and Houlsby, 1991; Chen and Abousleiman, 2013; Carter and Yu, 2022). With the axisymmetric assumption, the stress equilibrium equation in the radial direction can be expressed as

$$\frac{\mathrm{d}\sigma_r}{\mathrm{d}r} + \frac{(\sigma_r - \sigma_\theta)}{r} = 0 \tag{3}$$

where σ_θ is the circumferential stress, and $\mathrm{d}(\cdot)$ is the spatial differential of $(\cdot)$ for a given time (i.e. Eulerian description).

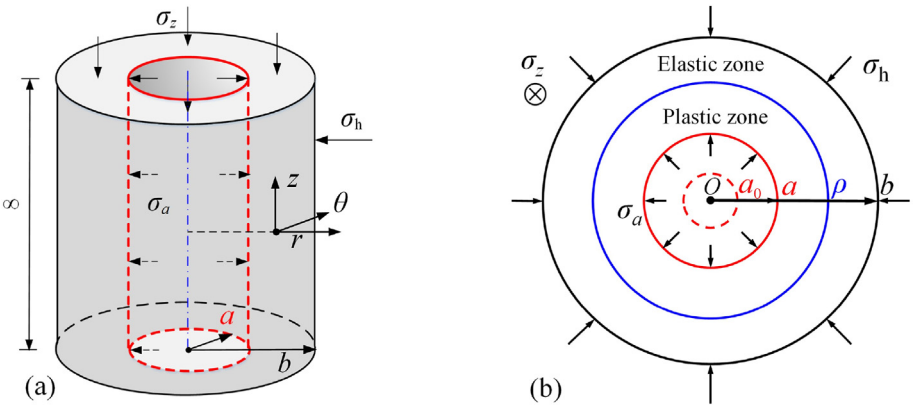

Fig. 1. Schematic of the cavity expansion problem: (a) Boundary conditions, and (b) Coordinate system.

Rigorous definitions of the two stress invariants, namely the mean effective stress and deviatoric stress (p, q), are followed as given in Eqs. (4) and (5):

$$p = \frac{1}{3}(\sigma_r + \sigma_\theta + \sigma_z) \tag{4}$$

$$q = \frac{1}{\sqrt{2}}\sqrt{(\sigma_r - \sigma_\theta)^2 + (\sigma_r - \sigma_z)^2 + (\sigma_\theta - \sigma_z)^2} \tag{5}$$

Then the conjugated volumetric strain (ε_v) is defined as

$$\varepsilon_v = \varepsilon_r + \varepsilon_\theta + \varepsilon_z \tag{6}$$

where ε_r, ε_θ, and ε_z denote the radial, circumferential, and vertical strains, respectively. Note here the vertical strain remains zero (i.e. $\varepsilon_z = 0$) for the present plane strain problem.

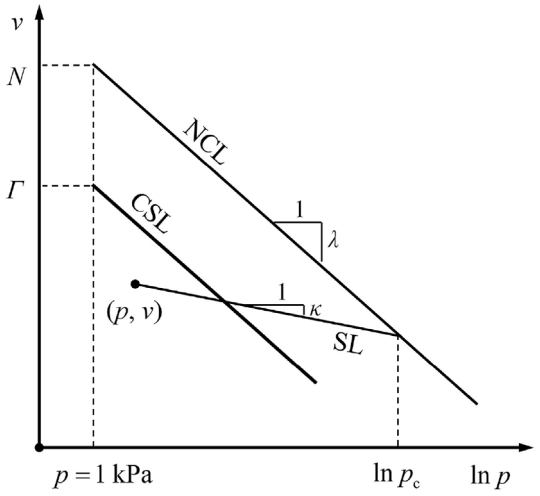

Fig. 2. Definitions of the model parameters.

3. Critical state soil models

Three widely-used critical state models are considered in this study to describe the soil behaviour, including the original Cam Clay model (OCC), the modified Cam Clay model (MCC), and the Clay and Sand model (CASM) (Yu, 1998). The reasons for choosing these typical models are primarily to: (i) show the general characteristic of the new solution in terms of different constitutive models; and (ii) make it convenient for practical use (e.g. validation of numerical methods). As shown in Fig. 2, the critical state line (CSL) and normal consolidation line (NCL) are parallel with each other in the v-ln$p$ plane with a slope of λ, and the specific volumes (v) at the intersection with $p = 1$ kPa are Γ and N, respectively. In the p-q plane, the slope of the CSL is denoted as M.

The swelling and recompression loop (i.e. reversible processes) is represented by a single straight line:

$$v = v_0 - \kappa \ln(p / p_0) \tag{7}$$

where v_0 denotes the initial specific volume; κ is the slope of the swelling line (SL) in the v-ln$p$ plane; and p_0 denotes the initial mean stress. The elastic modulus E can be expressed as

$$E(v, p) = 3(1 - 2\mu)vp/\kappa \tag{8}$$

where μ is the Poisson's ratio of the soil.

The yield function f and the plastic potential g for two-invariant Cam Clay soil models can be uniformly expressed as

$$f = f(p, q, p_c) = 0 \tag{9}$$

$$g = g\left(p, q, p_g\right) = 0 \tag{10}$$

where p_c and p_g are size parameters for the yield surface and plastic potential, respectively. p_{c0} is the initial value of p_c (Fig. 2). The evolution of p_c is controlled by the volumetric-hardening law:

$$\mathrm{D}\varepsilon_v^{\mathrm{p}} = \frac{\lambda - \kappa}{v}\frac{\mathrm{D}p_c}{p_c} \tag{11}$$

where $\varepsilon_v^{\mathrm{p}}$ denotes the plastic volumetric strain; $\mathrm{D}(\cdot)$ denotes the material time differential of $(\cdot)$ for a given soil material point (i.e. Lagrangian description). Expressions of the yield function f and the

Table 1
f and p_c for the selected Cam Clay models.

Model	$f(p,q,p_c)$	$p_c(p,q)$	Plastic flow rule
OCC	$\eta/M - \ln(p_c/p)$	$p\exp(\eta/M)$	Associated
MCC	$(\eta/M)^2 - (p_c/p - 1)$	$p[1 + (\eta/M)^2]$	Associated
CASM	$(\eta/M)^n - \frac{\ln(p_c/p)}{\ln r^*}$	$p\exp[\ln r^*(\eta/M)^n]$	Non-associated

Note: $\eta = q/p$ is the stress ratio; n and r^* are material constants of the CASM, which control the curvature of the yield surface and the intersection point of the CSL and the yield surface, respectively.

isotropic consolidation pressure p_c are summarised in Table 1 for the OCC, MCC, and CASM models.

4. Analytical solution for the elastic analysis

Soil deformation in the elastic zone (i.e. $\rho \leq r \leq b$) is usually very small so the small strain theory is commonly adopted in the elastic analysis (Yu and Houlsby, 1991; Chen and Abousleiman, 2013), by which the stress-strain relationship can be expressed as

$$\begin{bmatrix} \mathrm{D}\varepsilon_r^{\mathrm{e}} \\ \mathrm{D}\varepsilon_\theta^{\mathrm{e}} \\ \mathrm{D}\varepsilon_z^{\mathrm{e}} \end{bmatrix} = \begin{bmatrix} -\mathrm{d}(\mathrm{D}u)/\mathrm{d}r \\ -\mathrm{D}u/r \\ 0 \end{bmatrix} = \frac{1}{E(\nu,p)} \begin{bmatrix} 1 & -\mu & -\mu \\ -\mu & 1 & -\mu \\ -\mu & -\mu & 1 \end{bmatrix} \begin{bmatrix} \mathrm{D}\sigma_r \\ \mathrm{D}\sigma_\theta \\ \mathrm{D}\sigma_z \end{bmatrix} \tag{12}$$

where $\varepsilon_k^{\mathrm{e}}$ ($k = r, \theta, z$) denotes the elastic component of ε_k and is taken as positive for compression; and $u = r - r_0$ is the radial displacement of a soil material point whose initial radius is r_0. It is noted that Eq. (12) cannot be easily solved following conventional approaches (e.g. Yu, 1992) because the stress-dependent elastic moduli are influenced by the outer boundary effect. Elastic solutions for stresses and displacements should be discussed separately as follows.

4.1. Stress analysis

The compatibility equation in terms of strain components can be obtained from Eq. (12) (Salgado et al., 1997; Yu, 2000):

$$\frac{\mathrm{d}(\mathrm{D}\varepsilon_\theta^e)}{\mathrm{d}r} + \frac{(\mathrm{D}\varepsilon_\theta^e - \mathrm{D}\varepsilon_r^e)}{r} = 0 \tag{13}$$

Substituting Eq. (12) into Eq. (13), the compatibility equation will become

$$\frac{\mathrm{d}}{\mathrm{d}r}[-\mu\sigma_r + (1-\mu)\sigma_\theta] + \frac{\sigma_\theta - \sigma_r}{r} = 0 \tag{14}$$

Combination of Eqs. (3) and (14) leads to

$$\frac{\mathrm{d}}{\mathrm{d}r}(\sigma_r + \sigma_\theta) = 0 \tag{15}$$

It is interesting to find that $\sigma_r + \sigma_\theta$ does not vary with radial positions (but it may vary with time), and $\sigma_r + \sigma_\theta$ is denoted as $2\sigma_{\mathrm{h}} - B_\rho$ without loss of generality.

Then the elastic stresses can be readily obtained by solving Eqs. (2), (3), (12) and (15):

$$\sigma_r = \sigma_{\mathrm{h}} + B_\rho\left[(b/r)^2 - 1\right] \tag{16a}$$

$$\sigma_\theta = \sigma_{\mathrm{h}} - B_\rho\left[(b/r)^2 + 1\right] \tag{16b}$$

$$\sigma_z = \sigma_{\mathrm{v}} - 2\mu B_\rho \tag{16c}$$

$$B_\rho = \frac{\sigma_{r\rho} - \sigma_{\mathrm{h}}}{(b/\rho)^2 - 1} \tag{16d}$$

where $\sigma_{r\rho}$ denotes the radial stress at the elastic-plastic boundary ($r = \rho$); and B_ρ can be found to be a non-negative constant for a given time (but it changes with ρ or time).

The mean effective stress and deviatoric stress at $r = \rho$ (i.e. p_ρ and q_ρ) can be obtained by substituting Eq. (16) into Eqs. (4) and (5) with the unknown of B_ρ. Based on the stress continuity conditions at $r = \rho$, B_ρ can be determined by substituting p_ρ and q_ρ into yield function (9). Then the specific volume at $r = \rho$ (i.e. ν_ρ) can be computed from Eq. (7).

4.2. Displacement analysis

Eqs. (4) and (16) indicate the mean effective stress in the elastic zone varies during the expansion process. Accordingly, the elastic moduli of soils vary as they are assumed to be stress-dependent in these Cam Clay models. In this case the elastic displacement is written in an incremental form by combining Eqs. (12) and (16):

$$\mathrm{D}u = \frac{r(1+\mu)}{E(\nu,p)}\left[1 - 2\mu + (b/r)^2\right]\mathrm{D}B_\rho \tag{17}$$

An analytical solution for displacement analysis is innovatively developed as follows.

Combining Eqs. (4) and (16), the mean effective stress in the elastic zone can be expressed as

$$p = p_0 - \frac{2(1+\mu)}{3}B_\rho \tag{18}$$

where $p_0 = (\sigma_{\mathrm{v}} + 2\sigma_{\mathrm{h}})/3$ denotes the initial mean effective stress. Eq. (18) demonstrates that: (i) the mean effective stress is no longer a constant in the elastic zone due mainly to the influence of the outer boundary effect, which is different to published solutions for cavity expansion in the infinite soil mass (e.g. Chen and Abousleiman, 2013; Mo and Yu, 2018); and (ii) the mean effective stress is only dependent on time (or B_ρ), instead of varying with the radial position. The latter conclusion is essential to develop the analytical form of displacement solution.

For a soil material point in the elastic zone, the integral of Eq. (17) together with Eqs. (7), (8), (16) and (18) can give the integral form of particle displacements:

$$u(r) = \int_{p_0}^{p_\rho} \frac{-r\kappa}{2(1-2\mu)}\left[\frac{1 - 2\mu + (b/r)^2}{\nu_0 - \kappa\ln(p/p_0)}\right]\frac{\mathrm{D}p}{p} \tag{19}$$

Owing to the small strain assumption in the elastic zone, the current radial position of a particle can be replaced by its original position (i.e. $r = r_0$ and $b = b_0$) when calculating elastic displacements. Therefore, elastic displacements can be obtained by integrating Eq. (19) as

$$\frac{u(r)}{r_0} = \frac{1 - 2\mu + (b_0/r_0)^2}{2(1-2\mu)}\ln\left(1 - \frac{\kappa}{\nu_0}\ln\frac{p_\rho}{p_0}\right) \tag{20}$$

In particular, the displacements at the elastic-plastic boundary and the outer cylinder wall can then be obtained from Eq. (20) as

$$\frac{u(\rho)}{\rho_0} = \frac{1 - 2\mu + (b_0/\rho_0)^2}{2(1-2\mu)}\ln\left(1 - \frac{\kappa}{\nu_0}\ln\frac{p_\rho}{p_0}\right) \tag{21}$$

$$\frac{u(b)}{b_0} = \frac{1-\mu}{1-2\mu}\ln\left(1 - \frac{\kappa}{\nu_0}\ln\frac{p_\rho}{p_0}\right) \tag{22}$$

where ρ_0 is the initial value of ρ. An iteration can be made by replacing ρ_0 and b_0 in Eqs. (21) and (22) with the newly derived ρ and b, respectively, which will give rather accurate results of ρ and b.

Closed-form solutions for stresses and displacements in the elastic zone are presented by Eqs. ((7), (16), (18) and (20). The analytical expressions can greatly simplify calculation procedures

for the analysis in the elastic zone and provide the boundary values at $r = \rho$ for the PDEs in the plastic zone. In addition, these solutions can also be used for the calculation of stresses and displacements during the purely elastic expansion process (i.e. entire soil deforms elastically) by replacing ρ and $\sigma_{r\rho}$ with a and σ_a respectively.

5. Governing equations for plastic analysis

In this section five first-order PDEs are formulated to solve the unknowns (e.g. r, σ_r, σ_θ, σ_z, and v) required for the analysis in the plastic zone ($a \le r < \rho$), which is achieved by the combined use of Eulerian description (for a given time) and Lagrangian description (for a given particle) as follows.

At first, to account for the large deformation effect in the plastic zone, the Eulerian logarithmic strains are adopted (Chen and Abousleiman, 2013; Mo and Yu, 2018):

$$\varepsilon_r = -\ln(\mathrm{d}r/\mathrm{d}r_0) \tag{23}$$

$$\varepsilon_\theta = -\ln(r/r_0) \tag{24}$$

$$\varepsilon_v = -\ln(v/v_0) \tag{25}$$

The radial, circumferential, and volumetric strains are not independent and should satisfy Eq. (6), thereby giving the compatibility equation in terms of r and v:

$$\mathrm{d}r = \frac{vr_0}{rv_0}\mathrm{d}r_0 \tag{26}$$

Combining Eqs. (3) and (26), the stress equilibrium equation can be transformed to be the expression of σ_r in the Eulerian description:

$$\mathrm{d}\sigma_r = (\sigma_\theta - \sigma_r)\frac{vr_0}{rv_0}\mathrm{d}r_0 \tag{27}$$

Following Chen and Abousleiman (2012), the elastic-plastic constitutive equations can be written in the Lagrangian form:

$$\begin{bmatrix} \mathrm{D}\varepsilon_r \\ \mathrm{D}\varepsilon_\theta \\ \mathrm{D}\varepsilon_z \end{bmatrix} = \begin{bmatrix} A_{rr} & A_{r\theta} & A_{rz} \\ A_{\theta r} & A_{\theta\theta} & A_{\theta z} \\ A_{zr} & A_{z\theta} & A_{zz} \end{bmatrix} \begin{bmatrix} \mathrm{D}\sigma_r \\ \mathrm{D}\sigma_\theta \\ \mathrm{D}\sigma_z \end{bmatrix} \tag{28}$$

where A_{kl} ($k = r, \theta, z$; $l = r, \theta, z$) is defined as

$$A_{kl} = \begin{cases} -\dfrac{\mu}{E} + \dfrac{1}{K_\mathrm{p}}\dfrac{\partial g}{\partial \sigma_k}\dfrac{\partial f}{\partial \sigma_l}, k \neq l \\ \dfrac{1}{E} + \dfrac{1}{K_\mathrm{p}}\dfrac{\partial g}{\partial \sigma_k}\dfrac{\partial f}{\partial \sigma_k}, k = l \end{cases} \tag{29}$$

$$K_\mathrm{p} = -\frac{\partial f}{\partial p_\mathrm{c}}\frac{\partial g}{\partial p}\frac{vp_\mathrm{c}}{\lambda - \kappa} \tag{30}$$

Substituting Eqs. (6), (24) and (25) into Eq. (28), the circumferential stress, vertical stress, and specific volume can be expressed in the incremental form:

$$\begin{bmatrix} \mathrm{D}\sigma_\theta \\ \mathrm{D}\sigma_z \end{bmatrix} = \begin{bmatrix} A_{\theta\theta} & A_{\theta z} \\ A_{z\theta} & A_{zz} \end{bmatrix}^{-1} \begin{bmatrix} -A_{\theta r}\mathrm{D}\sigma_r - \mathrm{D}r/r \\ -A_{zr}\mathrm{D}\sigma_r \end{bmatrix} \tag{31}$$

$$\frac{\mathrm{D}v}{v} = -\begin{bmatrix} A_{rr} + A_{\theta r} + A_{zr} \\ A_{r\theta} + A_{\theta\theta} + A_{z\theta} \\ A_{rz} + A_{\theta z} + A_{zz} \end{bmatrix}^\mathrm{T} \begin{bmatrix} \mathrm{D}\sigma_r \\ \mathrm{D}\sigma_\theta \\ \mathrm{D}\sigma_z \end{bmatrix} \tag{32}$$

Five PDEs for the analysis in the plastic zone have been obtained by the combination use of Eulerian description (i.e. Eqs. (26) and (27)) and Lagrangian description (i.e. Eqs. (31) and (32)). Consequently, the stresses and strains in the plastic zone can be calculated with the information at the elastic-plastic boundary. It is noted that no specific constitutive models are restricted in the above derivations so that these equations can be useful for a wide range of materials. Taking the OCC, MCC, and CASM models as example, detailed expressions for K_p, $\partial g/\partial \sigma_k$, and $\partial f/\partial \sigma_k$ in Eq. (29) are summarised in Table 2.

In addition, the entire soil cylinder may become plastic or enter the fully plastic expansion stage. This is easy to occur when (i) The thickness ratio of the soil cylinder (b_0/a_0) is small; (ii) The initial overconsolidation ratio of soil (represented by $R_0 = p_{c0}/p_0$) is close to 1; and (iii) The cavity expansion level gets sufficiently large. In this case the above governing PDEs still work, but the boundary values at $r = \rho$ should be replaced by those at $r = b$.

6. Problem definition and assumptions

Both the material time derivative (Lagrangian description) and the spatial derivative (Eulerian description) are involved in the governing PDEs for the elastoplastic cavity expansion analysis, and they cannot be transformed into ODEs easily for the present non-self-similar problem, if not impossible. In this section, a novel solution algorithm for solving this problem is developed as follows.

It is convenient to discrete the hollow cylinder of soil into ($m-1$) concentric annuli, where m represents the number of nodes (Fig. 3). At the same time, the loading process is divided into a number of continuous load steps. In the step prior to loading (i.e. step (0)), each node is marked by its initial position $r_{(i)}^{(0)}$, where the subscript $i = 1, 2, 3, \ldots, m$ denotes the ith node and the superscript denotes the number of load step. To improve calculation efficiency, the distribution of nodes is set to follow the nonlinear function:

$$r_{(i+1)}^{(0)} = \left(\frac{b_0}{a_0}\right)^{1/(m-1)} r_{(i)}^{(0)} \tag{33}$$

For convenience, the radial location, as well as stress and deformation conditions, for the ith node at the jth load step is stored in an information vector:

Table 2
K_p, $\partial f/\partial \sigma_k$, and $\partial g/\partial \sigma_k$ for the selected Cam Clay models.

Model	Functions
OCC	$K_\mathrm{p} = \frac{v}{\lambda-\kappa}\frac{M-\eta}{Mp}$, $\frac{\partial f}{\partial \sigma_k} = \frac{\partial g}{\partial \sigma_k} = \frac{M-\eta}{3Mp} + \frac{3(\sigma_k - p)}{2Mpq}$
MCC	$K_\mathrm{p} = \frac{v}{\lambda-\kappa}\frac{M^4-\eta^4}{M^4p}$, $\frac{\partial f}{\partial \sigma_k} = \frac{\partial g}{\partial \sigma_k} = \frac{M^2-\eta^2}{3M^2p} + \frac{3(\sigma_k - p)}{M^2p^2}$
CASM	$K_\mathrm{p} = \frac{v}{\lambda-\kappa}\frac{1}{\ln r^*}\frac{27(M-\eta)}{p(3+2\eta)(3-\eta)}$, $\frac{\partial f}{\partial \sigma_k} = \frac{1-n\ln r^*(\eta/M)^n}{3(\ln r^*)p} + \frac{3(\sigma_k - p)n\eta^{n-1}}{2M^nqp}$, $\frac{\partial g}{\partial \sigma_k} = \frac{9[M-\eta+(9+3M-2M\eta)(\sigma_k - p)/2q]}{p(3+2\eta)(3-\eta)}$

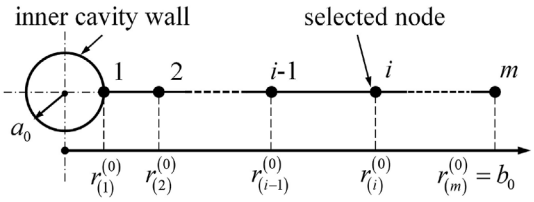

Fig. 3. Discretisation of calculation nodes.

$$\boldsymbol{x}_{(i)}^{(j)} = \left[r_{(i)}^{(j)}, \sigma_{r_{(i)}}^{(j)}, \sigma_{\theta(i)}^{(j)}, \sigma_{z(i)}^{(j)}, v_{(i)}^{(j)}\right]^{\mathrm{T}} \tag{34}$$

where the superscript "(j)" represents the jth load step.

The loading process is controlled by gradually increasing the radius of the elastic-plastic boundary. A special loading pattern that the elastic-plastic boundary expands to the jth node at the end of the jth load step (i.e. $\rho_0^{(j)} = r_{(j)}^{(0)}$ and $\rho^{(j)} = r_{(j)}^{(j)}$), is chosen to connect the integrations with respect to time (for a given particle) and space (for a given time). Therefore, the calculation of $\boldsymbol{x}_{(i)}^{(j)}$ can be divided into three cases (Fig. 4a):

(1) If (j)<(i), the ith node is within the elastic zone, which means $\boldsymbol{x}_{(i)}^{(j)}$ can be readily derived from the elastic solution;
(2) If (j)=(i), the ith node is just on the elastic-plastic boundary. In this case, $\boldsymbol{x}_{(j)}^{(j)}$ can also be determined by the elastic solution with $r_0 = \rho_0^{(j)} = r_{(j)}^{(0)}$;
(3) If (j)>(i), the ith node is within the plastic zone and then $\boldsymbol{x}_{(i)}^{(j)}$ needs to be calculated by solving the governing PDEs in the plastic zone.

Fig. 4b shows the increments of $\boldsymbol{x}$ with respect to time and space (i.e. D$\boldsymbol{x}$ and d$\boldsymbol{x}$) for the elastoplastic cavity expansion analysis. At the jth load step, the increment of $\boldsymbol{x}$ from node (i+1) to node (i) is defined as

$$\mathrm{d}\boldsymbol{x} = \boldsymbol{x}_{(i)}^{(j)} - \boldsymbol{x}_{(i+1)}^{(j)} \tag{35}$$

The explicit Euler method is chosen to solve the PDEs. Specifically, dr and dσ_r can be obtained from Eqs. (26), (27) and (35) with the known information of $\mathrm{d}r_0 = r_{(i)}^{(0)} - r_{(i+1)}^{(0)}$ and $\boldsymbol{x} = \boldsymbol{x}_{(i+1)}^{(j)}$, and then $r_{(i)}^{(j)}$ and $\sigma_{r_{(i)}}^{(j)}$ are determined. $\boldsymbol{x}_{(i+1)}^{(j)}$ with decreasing node numbers can be determined node-by-node from the elastic-plastic boundary to the inner cylinder wall (i.e. from node $r_{(j)}^{(j)}$ to node $r_{(1)}^{(j)}$).

For the ith node upon loading from load step (j-1) to load step (j), D$\boldsymbol{x}$ is equal to

$$\mathrm{D}\boldsymbol{x} = \boldsymbol{x}_{(i)}^{(j)} - \boldsymbol{x}_{(i)}^{(j-1)} \tag{36}$$

where $\boldsymbol{x}_{(i)}^{(j-1)}$ is known from the previous step of loading. Having calculated $r_{(i)}^{(j)}$ and $\sigma_{r_{(i)}}^{(j)}$ from Eqs. (26), (27) and (35), D$r_{(i)}^{(j)}$ and D$\sigma_{r_{(i)}}^{(j)}$ can be known by Eq. (36). Then, Dσ_θ, Dσ_z, and Dv can be calculated from Eqs. (31), (32) and (36) with $\boldsymbol{x} = \boldsymbol{x}_{(i)}^{(j-1)}$, and $\sigma_{\theta(i)}^{(j)}$, $\sigma_{z(i)}^{(j)}$, and $v_{(i)}^{(j)}$ are also determined. By repeating the above work until a target expansion level is reached (e.g. the inner radial reaches a_{end}), stresses and displacements during the continuous expansion process can be computed, and the calculation procedures are summarised in Fig. 5.

7. Special cases

In this section, the adaptability of the present solution approach is further discussed taking two special cases as examples.

7.1. Self-similar cavity expansion problem

Assuming the outer radius of the soil cylinder to be infinite (i.e. $b_0/a_0 = \infty$), the cavity may expand in a self-similar manner. In this simplified case, all material points follow exactly the same and unique stress/deformation path during the expansion process, which implies that all the stress components and specific volume for any material point, could be functions of one single variable (e.g. ε_θ) (Chen and Abousleiman, 2013). On this basis, the preceding governing PDEs in terms of time and spatial derivatives can be transformed into a set of ODEs by introducing an appropriate timescale or auxiliary variable. Normally, the auxiliary variable χ is the monotonic function of a dimensionless radial coordinate which satisfies the equality relation of dχ = Dχ, for example, r/ρ, $(r - r_0)/r$, and r_0/r (Collins et al., 1992; Chen and Abousleiman, 2013; Su, 2021). The connection between the present method and the auxiliary variable approach is discussed as follows.

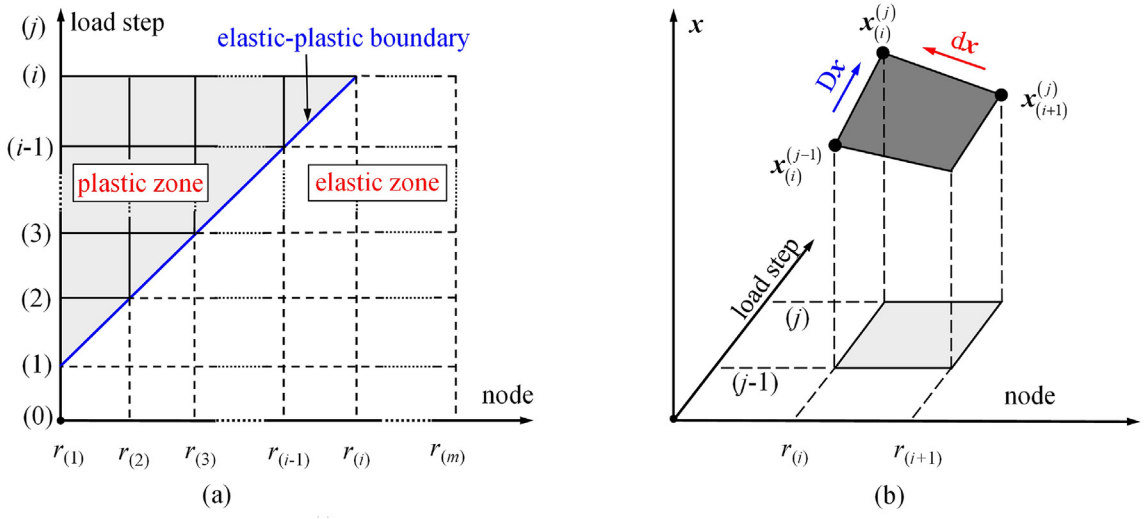

Fig. 4. $\boldsymbol{x}_{(i)}^{(j)}$: (a) Two-dimensional schematic, and (b) Three-dimensional schematic.

1 Input initial parameters, including:
- 1.1 Soil parameters (Γ, λ, κ, μ, M, n, and r^*) and stress state (σ_h, σ_v, and R_0);
- 1.2 Shape parameters (a_0, b_0, and a_{end});
- 1.3 m that controls the node numbers.

2 Calculate p_0, q_0, p_{c0}, and v_0; calculate $r_{(i)}^{(0)}$ by Eq. (33).

3 Calculate the purely elastic loading response:
- 3.1 Gradually increase σ_a ($\sigma_a > \sigma_h$) until initial yielding occurs;
- 3.2 Calculate the stresses by Eq. (16) with $\sigma_{r\rho} = \sigma_a$ and $a = \rho$;
- 3.3 Calculate the p, q, and v by Eqs. (4), (5), and (7), respectively;
- 3.4 Calculate the particle displacement u by Eq. (20).

4 Calculate the elastic-plastic loading response ($\rho_0^{(j)} < b_0$):
- 4.1 Let $(j)=(i)=1$ and $\rho_0^{(j)} = r_{(1)}^{(0)} = a_0$;
- 4.2 Calculate B_ρ by numerically solving Eqs. (4), (5), (9) and (16);
- 4.3 Calculate $\boldsymbol{x}_{(1)}^{(1)}$ from Eqs. (7), (16), (18), and (20) with the known B_ρ;
- 4.4 If $a < a_{end}$
  - 4.4.1 Gradually increase (j) (i.e. $(j)=(j)+1$); $\rho_0^{(j)} = r_{(j)}^{(0)}$;
  - 4.4.2 Calculate $\boldsymbol{x}_{(j)}^{(j)}$ following procedures 4.2 to 4.3;
  - 4.4.3 Calculate $\boldsymbol{x}_{(i)}^{(j)}$ node by node from $r_{(j)}^{(j)}$ to $r_{(1)}^{(j)}$ (i.e. (i) decreases from (j) to (1)); at each node, $\boldsymbol{x}_{(i)}^{(j)}$ is determined by:
    - calculate dr and dσ_r (then $r_{(i)}^{(j)}$ and $\sigma_{r(i)}^{(j)}$) from Eqs. (26) and (27);
    - calculate Dr and Dσ_r from Eq. (36);
    - calculate Dσ_θ and Dσ_z (then $\sigma_{\theta(i)}^{(j)}$ and $\sigma_{z(i)}^{(j)}$) from Eq. (31);
    - calculate Dv (then $v_{(i)}^{(j)}$) from Eq. (32);
- 4.5 End.

5 Calculate the fully plastic loading response ($\rho_0^{(j)} = b_0$):
- 5.1 $(j)=(i)=m$; $\rho_0^{(m)} = r_{(m)}^{(0)} = b_0$;
- 5.2 Calculate $\boldsymbol{x}_{(i)}^{(j)}$ following procedures 4.4.2 to 4.4.3;
- 5.3 If $a < a_{end}$
  - 5.3.1 Gradually increase (j) from (m); $r_{(m)}^{(j)}$ increases from $r_{(m)}^{(m)}$ ($r_{(m)}^{(j)} > r_{(m)}^{(m)}$).
  - 5.3.2 $\sigma_{r(m)}^{(j)} \equiv \sigma_h$; calculate $\sigma_{\theta(m)}^{(j)}$, $\sigma_{z(m)}^{(j)}$, and $v_{(m)}^{(j)}$ from Eqs. (31) and (32);
  - 5.3.3 Calculate $\boldsymbol{x}_{(i)}^{(j)}$ following procedure 4.4.3;
- 5.4 End.

6 At the final load step, iterate $\rho_0^{(j)}$ in procedure 4 (or $r_{(m)}^{(j)}$ in procedure 5) by the dichotomous method until $a \approx a_{end}$.

Fig. 5. Calculation procedures for the elastic-plastic cavity expansion response.

Following the above criteria, we can take $\chi = -\varepsilon_\theta$ (i.e. $\ln(r/r_0)$) as a new auxiliary variable to link loading history for a material point and field distribution for a given time. Then $D\varepsilon_\theta = d\varepsilon_\theta$ gives

$$\frac{dr_0}{r_0} = \frac{dr - Dr}{r} \tag{37}$$

Combining Eqs. (26) and (37), the term dr/r can be expressed by Dr/r as

$$\frac{dr}{r} = \left(\frac{r_0^2 v}{r_0^2 v - r^2 v_0}\right) \frac{Dr}{r} \tag{38}$$

With Eq. (38), the stress equilibrium equation (Eq. (3)) can be converted into the expression of σ_r in the Lagrangian form. As a result, the preceding PDEs for Dσ_r, Dσ_θ, Dσ_z, and Dv have been reduced to four ODEs in terms of Dr/r (i.e. $-D\varepsilon_\theta$), which can be readily solved using commercial ODE solvers. Therefore, the auxiliary variable approach can be seen as a special case of the present approach when $b_0/a_0 \to \infty$ and $\chi = -\varepsilon_\theta$.

7.2. Solution in elastic-perfectly plastic MC materials

The proposed solution method can also be extended to the expansion analysis of a pressurised cylinder with the elastic-perfectly plastic Mohr-Coulomb model, which has also been

investigated by Yu (1992) using the total strain approach. Necessary modifications for corresponding equations are given as follows.

As constant elastic moduli of soils were adopted in Yu (1992), expressions for the specific volume and displacement, corresponding to Eqs. (7) and (20), become

$$\frac{v_0}{v} = 1 + \frac{3(1-2\mu)(p-p_0)}{E_0} \tag{39}$$

$$\frac{u(r)}{r_0} = \frac{B_p(1+\mu)}{E_0}\left[1-2\mu+(b_0/r_0)^2\right] \tag{40}$$

where E_0 is the constant elastic modulus.

The yield function and plastic potential for the non-associated Mohr-Coulomb model are

$$f = \sigma_r - \frac{1+\sin\varphi}{1-\sin\varphi}\sigma_\theta - \frac{2c\cos\varphi}{1-\sin\varphi} = 0 \tag{41}$$

$$g = \sigma_r - \frac{1+\sin\psi}{1-\sin\psi}\sigma_\theta - \frac{2c\cos\psi}{1-\sin\psi} = 0 \tag{42}$$

where φ, c, and ψ denote the friction angle, cohesion, and dilation angle. Then the PDEs for $\mathrm{D}\sigma_\theta$, $\mathrm{D}\sigma_z$, and $\mathrm{D}v$ (i.e. Eqs. (31) and (32)) can be simplified as

$$\begin{bmatrix}\mathrm{D}\sigma_\theta\\ \mathrm{D}\sigma_z\end{bmatrix} = \frac{\mathrm{D}\sigma_r}{1+\sin\varphi}\begin{bmatrix}1-\sin\varphi\\ 2\mu\end{bmatrix} \tag{43}$$

$$\frac{\mathrm{D}v}{v} = C_\psi\frac{\mathrm{D}r}{r} + \frac{1}{E_0}\begin{bmatrix}2\mu-1-\mu C_\psi\\ 2\mu-1+C_\psi\\ 2\mu-1-\mu C_\psi\end{bmatrix}^{\mathrm{T}}\begin{bmatrix}\mathrm{D}\sigma_r\\ \mathrm{D}\sigma_\theta\\ \mathrm{D}\sigma_z\end{bmatrix} \tag{44}$$

where $C_\psi = (2\sin\psi)/(1+\sin\psi)$ is a material constant.

Yu and Houlsby (1991) and Yu (1992) demonstrated that σ_r and σ_θ can be directly obtained by combining the equilibrium equation and yield function (Eqs. (3) and (41)) with the perfectly elastic-plastic Mohr-Coulomb model (constant E_0, φ, c, and ψ). Following the loading history of a soil material point, Eqs. (43) and (44) can be analytically integrated to derive the expressions of $(v-v_0)$ and $(\sigma_z-\sigma_v)$ in terms of σ_r and σ_θ, which allows the cavity expansion analysis to be conducted by the total strain approach. Therefore, the analytical solution derived in Yu (1992) by the total strain approach can be seen as a special case of the present semi-analytical solution with state-independent strength, stiffness, and dilatancy.

8. Results and discussion

8.1. Solution validation

The proposed solution method is validated by comparison with some published results in the references. At first, the present solution is compared with the large strain solution of Yu (1992) for cavity expansion in a finite Mohr-Coulomb material, taking the same soil parameters ($E_0/(\alpha-1)=500\,\sigma_h$, $\mu=0.3$, $c=0$, $\varphi=40°$, and $\psi=0°$ and 20°). Fig. 6 shows that identical results are obtained by these two methods, which validates the accuracy of the proposed solution in this special case. The results also indicate that the outer boundary may impose a significant effect on the cavity expansion behaviour when the thickness ratio of the cylinder is smaller than a limit value, and this effect is enhanced in the soil with a larger dilation angle.

Using the auxiliary variable method, Chen and Abousleiman (2013) developed a rigorous drained solution for a cylindrical cavity expanding in an infinite soil mass adopting the MCC model. A comparison is made between Chen and Abousleiman's solution and the proposed solution with a sufficiently large value of b_0/a_0 (e.g. 10,000), taking the same input parameters as summarised in Table 3. In Figs. 7–9, the distributions of σ_r, σ_θ, and σ_z at $a_{end}/a_0=2$ are plotted in a semi-logarithmic scale, while the corresponding stress paths for a material point at $r_0=a_0$ are presented in the $p-q$ plane. It can be found that Chen and Abousleiman's solution can be exactly recovered by the present solution when $b_0/a_0\to\infty$. The good agreement also means that simplifying r by r_0 for displacements in the elastic zone (see Eq. (20)) can satisfy the calculation accuracy because of the sufficiently small strain.

Finally, the new solution is validated by comparison with FEM with the same input parameters in Table 3. The one-dimensional axisymmetric numerical model proposed by Zhou et al. (2021) is followed in the numerical simulations with Abaqus 2019. The

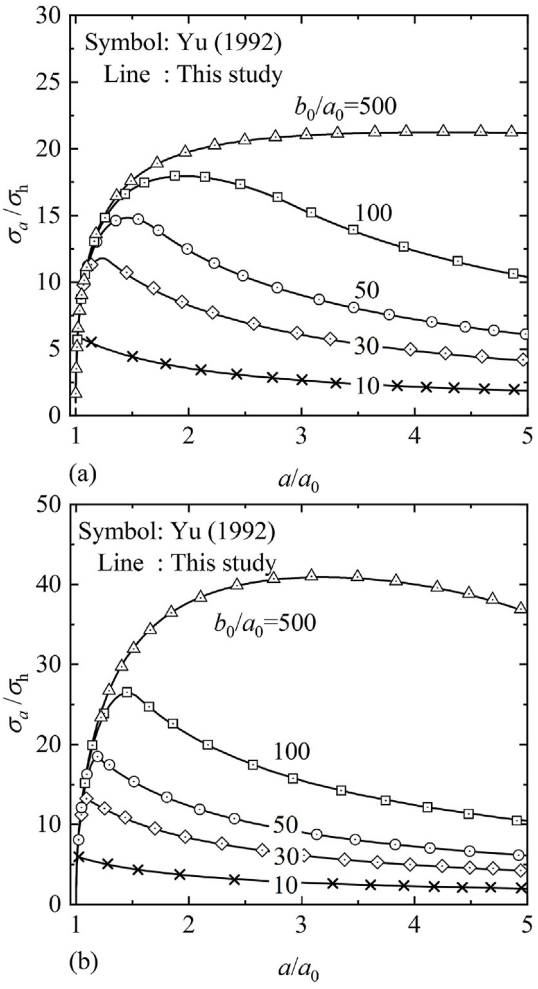

Fig. 6. Cavity expansion curves with various b_0/a_0 values: (a) $\psi=0°$ and (b) $\psi=20°$.

Table 3
Parameters used for the comparison with Chen and Abousleiman (2013).

R_0	σ_h (kPa)	σ_v (kPa)	p_0 (kPa)	q_0 (kPa)	σ_h/σ_v	v_0
1	100	160	120	60	0.625	2.09
3	120	120	120	0	1	1.97
10	144	72	120	72	2	1.80

Note: MCC model parameters are: $M=1.2$, $\lambda=0.15$, $\kappa=0.03$, $\mu=0.278$, and $\Gamma=2.74$. q_0 is the initial deviatoric stress.

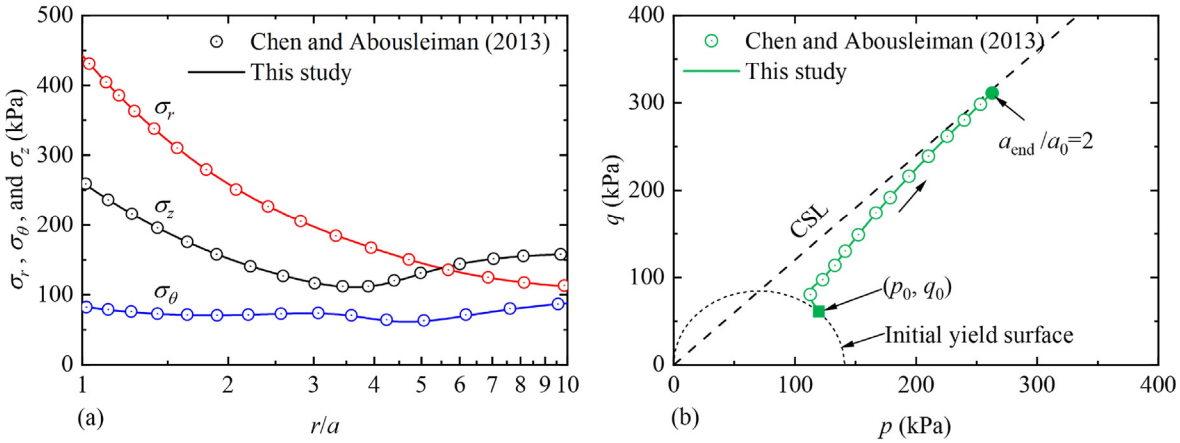

Fig. 7. Stress distributions and stress paths for $R_0 = 1$: (a) Stress distributions, and (b) Stress paths at the inner cavity wall.

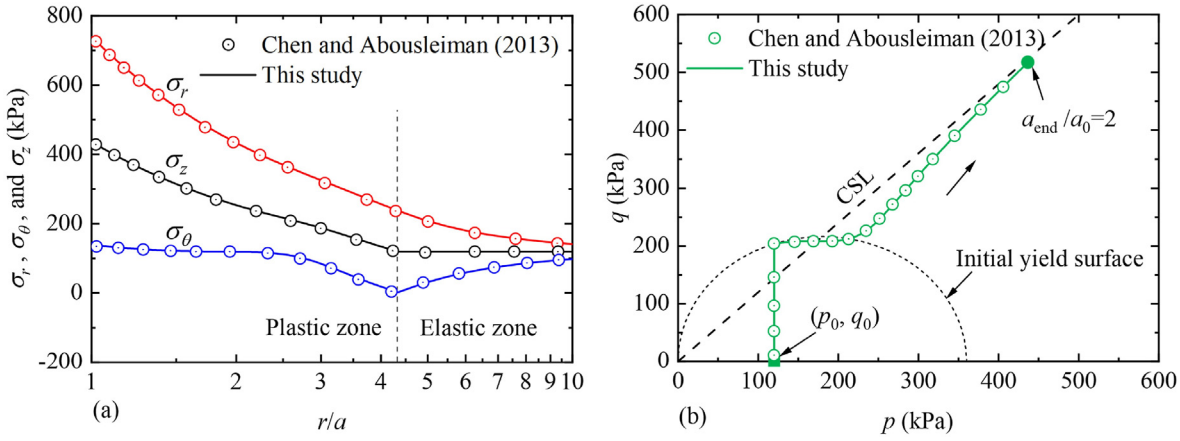

Fig. 8. Stress distributions and stress paths for $R_0 = 3$: (a) Stress distributions, and (b) Stress paths at the inner cavity wall.

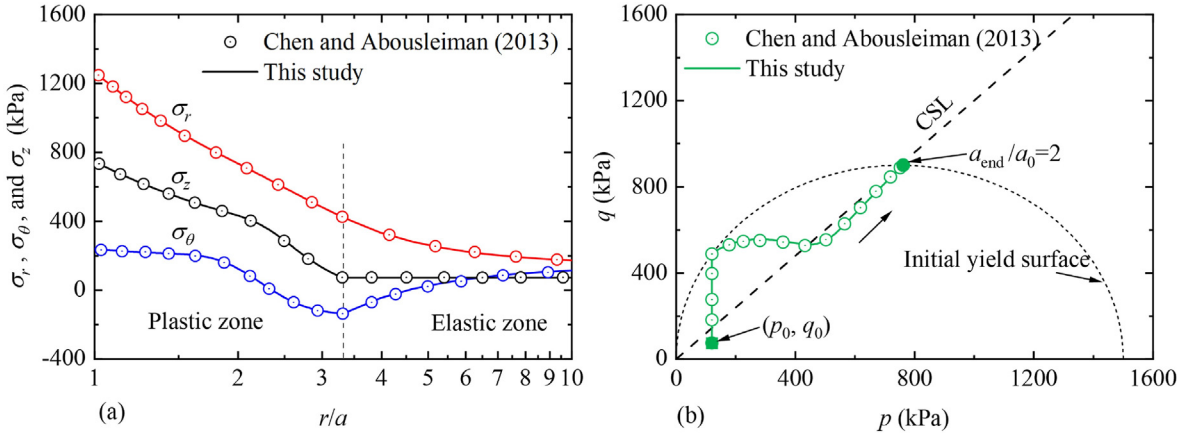

Fig. 9. Stress distributions and stress paths for $R_0 = 10$: (a) Stress distributions, and (b) Stress paths at the inner cavity wall.

thickness ratio b_0/a_0 is set as 20 and the MCC model built-in Abaqus is adopted. Fig. 10 shows the comparison of cavity expansion curves calculated by the present solution and FEM, and the identical results once again validate the soundness of the present solution.

8.2. Non-self-similar cavity expansion behaviour

For comparison, stress and deformation paths of soil material points at different radial positions (e.g. $r_0 = a_0$, $5a_0$, $15a_0$, and $30a_0 = b_0$) are captured during the expansion process. The results are plotted both in the $p - q$ and $v - \ln p$ planes as shown in

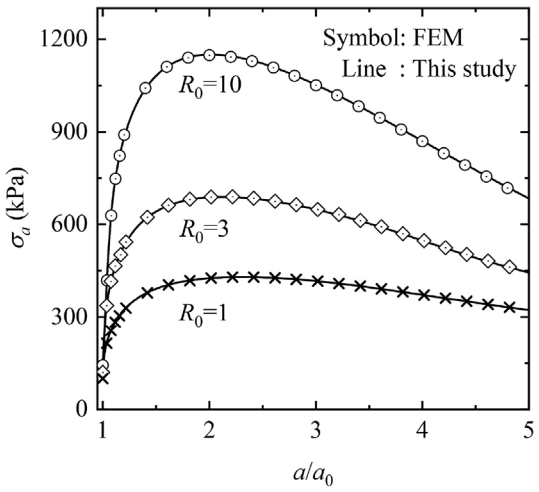

Fig. 10. Comparison of cavity expansion curves calculated by the present solution and FEM.

Figs. 11–13, in which the solid squares and circles mark the origin and end of loading (i.e. $a_{end}/a_0 = 5$), respectively.

During the continuous expansion process, it is known that all material points around the cavity share the same stress and deformation paths for self-similar cavity expansion problems (e.g. a cylindrical cavity in an infinite soil mass of axisymmetric stress conditions) (Collins et al., 1992; Chen and Abousleiman, 2013; Mo and Yu, 2018). On the contrary, Figs. 11–13 show that these paths differ significantly for particles at different radial positions, which corroborates the non-self-similar nature of cavity expansion in soils with a finite radial extent.

For the present non-self-similar problem, the stress states of soil material points closely relate to the level of expansion, the radial distance to the cavity wall, and the initial overconsolidation ratio. Figs. 11–13 indicate the closer to the cavity wall the earlier the stress state reaches the critical state, and soil material points with larger initial radii generally take shorter paths to the CSL. With the same expansion level, material points near the outer boundary may enter the plastic state in normally consolidated soils (e.g. $R_0 = 1$), whereas only elastic deformation occurs (e.g. within the initial yield surface in the $p - q$ plane or purely move along the SL in the $v - \ln p$ plane) in overconsolidated soils (e.g. $R_0 = 3$ and 10). The stress paths prior to yielding are approximately straight lines in the $p - q$ plane but vary with the radial positions of material points. In the purely elastic stage, the mean stress reduces upon loading, and the reduction becomes greater as the particle radius increases. This is also greatly different to what happens in a self-similar cavity expansion process (Chen and Abousleiman, 2013; Mo and Yu, 2018).

8.3. Cavity expansion response

Using the proposed solution for the MCC model with the parameters in Table 3, cavity expansion curves (i.e. σ_a/σ_h versus a/a_0) and stress paths of material points at the inner cavity wall with various b_0/a_0 ratios and R_0 values are calculated and plotted in Figs. 14–16. In these figures, the triangles on some cavity expansion curves indicate the moment that the elastic-plastic boundary just reaches the outer boundary of the hollow cylinder (i.e. $\rho_0 = b_0$), and the solid circle marks the end moment of loading (i.e. $a_{end}/a_0 = 5$). From the cavity expansion curves in Figs. 14–16, it can be seen: (i) With a large value of b_0/a_0, the required cavity pressure increases with a/a_0 and gradually approaches a limit pressure, which is almost the same as that happens for a cavity in an infinite soil mass; and (ii) When b_0/a_0 is small (e.g. less than 20 with the present parameters), a maximum cavity pressure may be reached, whereas this value could be much smaller than the aforementioned limit pressure, and the cavity pressure drops in the following expansion process.

The outer boundary effect becomes more significant with the increase of the overconsolidation ratio of soil (i.e. R_0). For example, for $a_{end}/a_0 = 5$, the inner cavity pressure for $b_0/a_0 = 30$ is 84.3 % of that for $b_0/a_0 \to \infty$ in the case of $R_0 = 1$, and this ratio becomes 76.8 % and 70.7 % in the cases of $R_0 = 3$ and 10, respectively. The outer boundary effect can also be clearly shown in the stress path plot (e.g. Fig. 14b, 15b and 16b). Initially, the stresses (p, q) with various b_0/a_0 values take almost the same paths to the CSL. With further expansion, the stresses keep increasing and finally approach a limit point on or near the CSL ($q/p \to M$ and $Dq/Dp \to M$) for the cases with $b_0/a_0 \to \infty$, while the stress path may reverse and reduce alone/near the CSL for the cases with a small b_0/a_0 ratio.

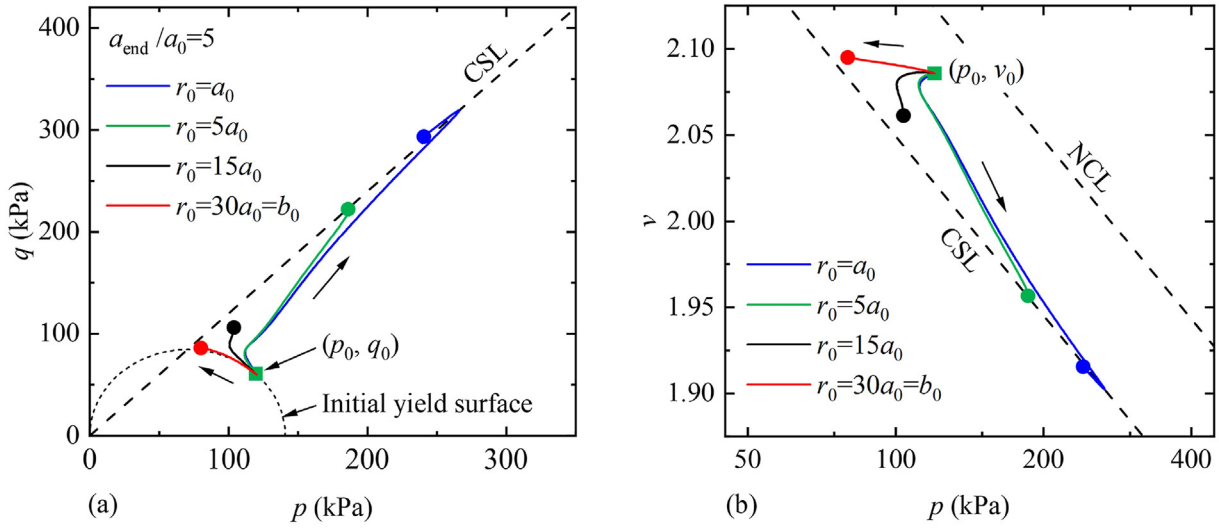

Fig. 11. Stress paths of various soil particles for $R_0 = 1$: (a) p-q plane, and (b) v-ln$p$ plane.

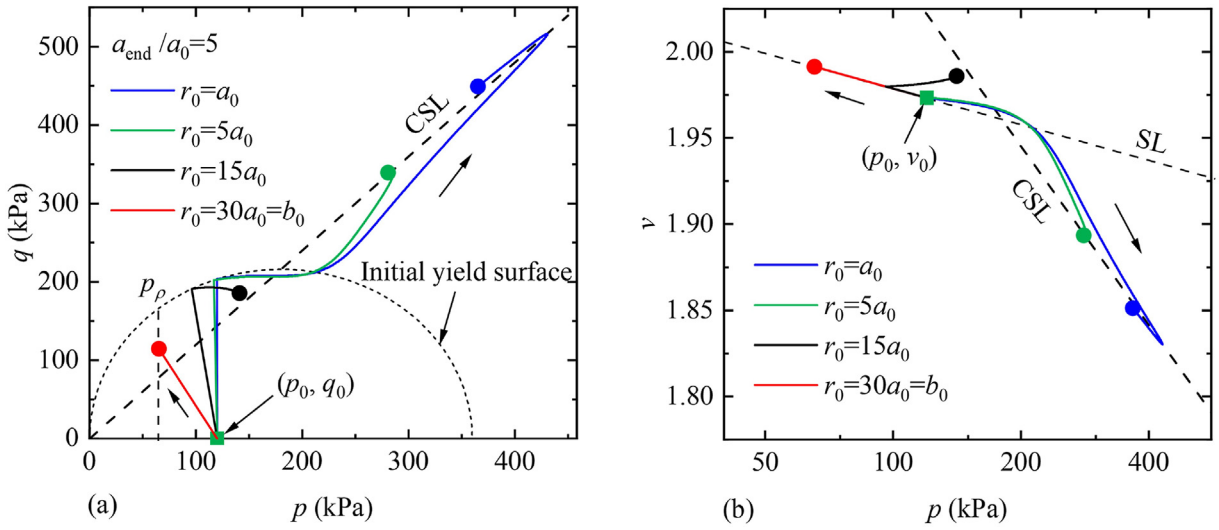

Fig. 12. Stress paths of various soil particles for $R_0 = 3$: (a) p-q plane, and (b) v-ln$p$ plane.

The turning point in the p-q plane gets earlier (i.e. smaller values of p and q) with the decrease of b_0/a_0.

Finally, to further highlight the significance of the new approach for non-self-similar cavity expansion problems, a comparison is made between the present exact solution and the approximate solution derived by the self-similar-based auxiliary variable approach. To adopt the auxiliary variable approach to the analysis of cavity expansion in the finite soil mass, three simplifying assumptions are required, including: (i) The loading history of soil material points and their spatial variations could be linked by an auxiliary variable, which was in fact based on the self-similar assumption; (ii) The radius ratio of the elastic-plastic boundary to the outer cylinder boundary (i.e. ρ/b) could be given as a constant during the loading process, which implies the cavity expansion behaviour is independent of b_0/a_0; and (iii) The soil cylinder would not enter the fully plastic expansion stage (i.e. $\rho_0/b_0 < 1$).

Figs. 17 and 18 show the comparison results calculated by the two approaches, taking parameters in Table 3 for the MCC model. In the approximate solution, ρ_0/b_0 is assumed to be 0.8 for cavity expansion in a finite soil mass and to be 0 for the infinite. As expected, Figs. 17 and 18 show that the approximate solution and the exact solution predict identical results while taking the cylinder thickness as infinite (i.e. $b_0/a_0 \to \infty$ and $\rho_0/b_0 = 0$). On the other hand, significant differences in cavity expansion curves and stress paths are observed once a finite soil mass ($b_0/a_0 = 20$) is considered. The exact solution predicts that the cavity pressure increases first and then drops after reaching a peak pressure. However, the approximate solution with a constant value of $\rho_0/b_0 = 0.8$ predicts that the inner pressure increases continually and finally approaches a limit pressure which is smaller than that for the case neglecting the finite boundary effect. This is primarily because ρ_0/b_0 should in reality increase from a_0/b_0 to 1, and constant ρ_0/b_0 in the approximate solution cannot account for the increasingly significant outer boundary effect during the continuous expansion process. Regarding the stress paths, the mean effective stress calculated by the approximate solution drops much faster than that by the exact solution in the elastic expansion stage and then approaches a steady state without softening. Overall, the auxiliary variable approach with the above simplifying assumptions may lead to considerable errors for the drained expansion

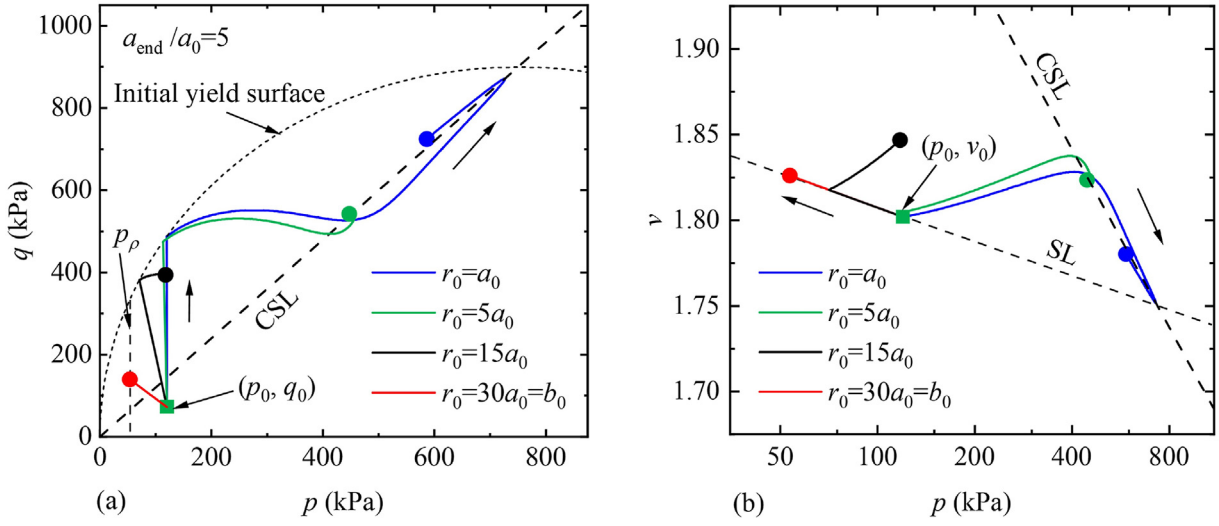

Fig. 13. Stress paths of various soil particles for $R_0 = 10$: (a) p-q plane, and (b) v-ln$p$ plane.

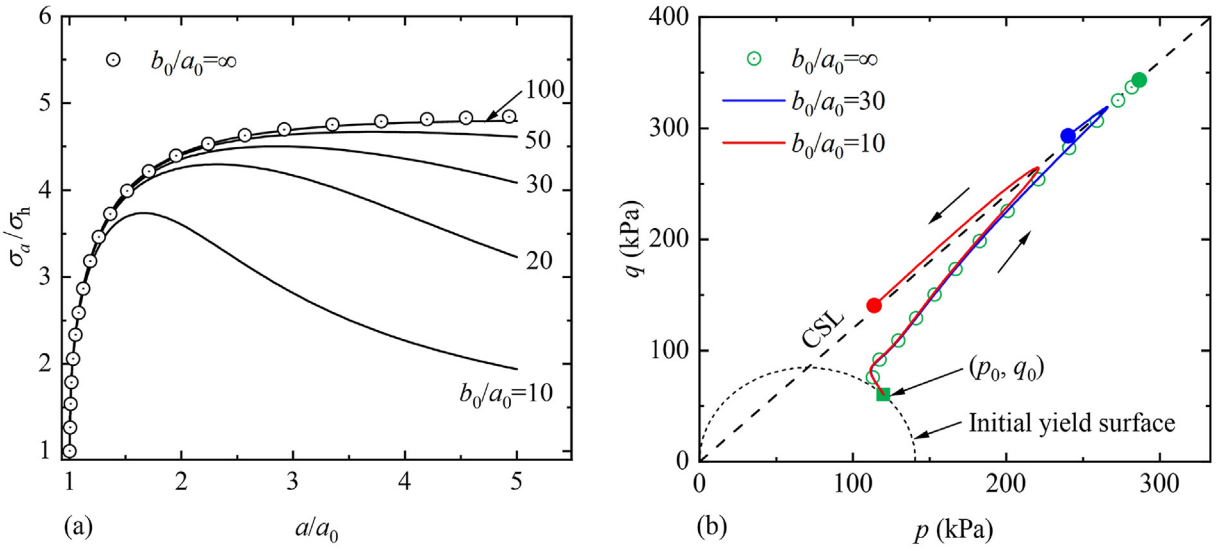

Fig. 14. Cavity expansion curves and stress paths at cavity wall for $R_0 = 1$: (a) Cavity expansion curves, and (b) Stress paths.

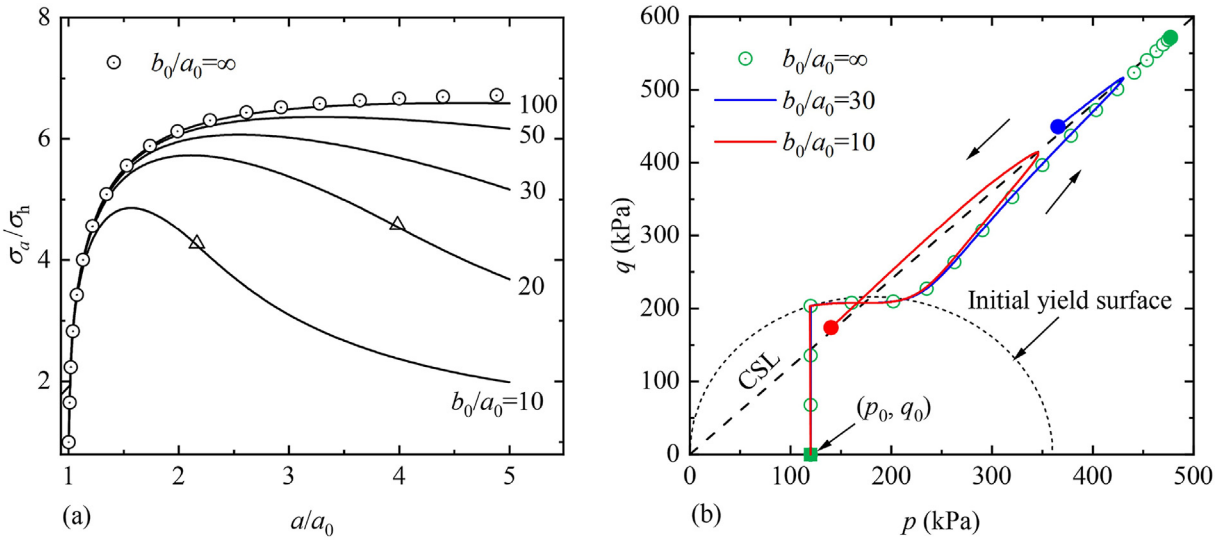

Fig. 15. Cavity expansion curves and stress paths at cavity wall for $R_0 = 3$: (a) Cavity expansion curves, and (b) Stress paths.

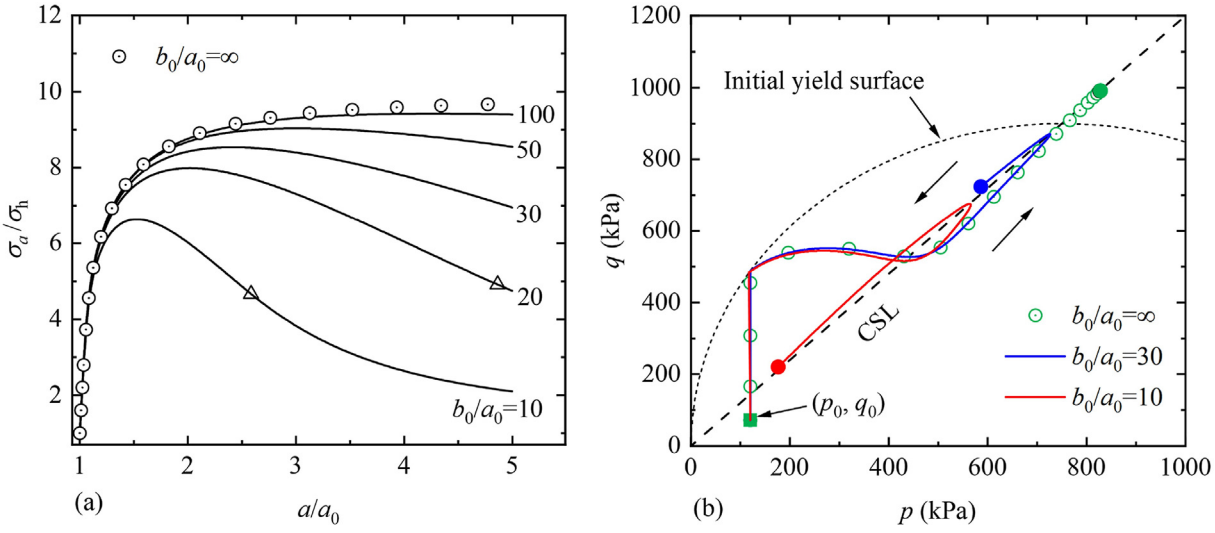

Fig. 16. Cavity expansion curves and stress paths at cavity wall for $R_0 = 10$: (a) Cavity expansion curves, and (b) Stress paths.

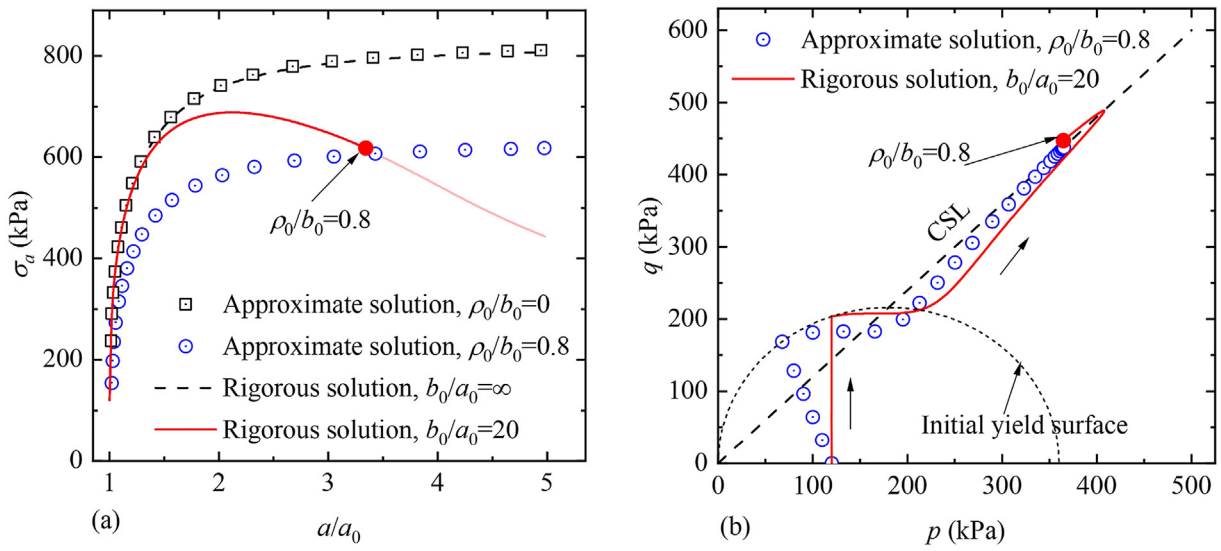

Fig. 17. Cavity expansion curves and stress paths at cavity wall for $R_0 = 3$: (a) Cavity expansion curves, and (b) Stress paths.

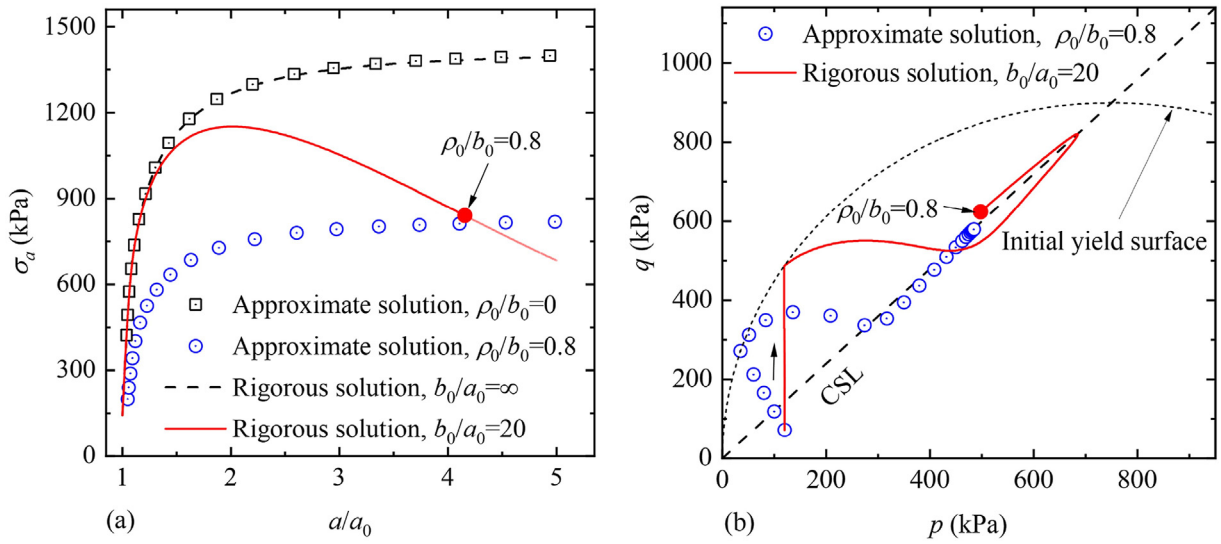

Fig. 18. Cavity expansion curves and stress paths at cavity wall for $R_0 = 10$: (a) Cavity expansion curves, and (b) Stress paths.

analysis of a thick-walled hollow cylinder of soils (i.e. non-self-similar problems).

9. Conclusions

This paper presents a novel semi-analytical solution for rigorous drained expansion of a pressurised cylinder of critical state soils. Considering stress-dependent soil moduli, an analytical solution for the elastic displacement is developed with the small strain assumption. For the large strain elastoplastic analysis, a set of first-order PDEs is constructed based on the combination use of Eulerian and Lagrangian descriptions, and an efficient solution algorithm is proposed for calculating stresses and deformation in the plastic zone. Simplifying $b_0/a_0 \to \infty$, solutions for corresponding cavity expansion problems in an infinite soil can be recovered by the present solution. It is also shown the new solution method has wider adaptability than the commonly used total strain method and auxiliary variable method.

Parametric analyses indicate that the outer boundary effect may significantly affect the cavity expansion response while b_0/a_0 is small, and this effect may become more significant with the increase of the expansion level a_{end}/a_0 and the overconsolidation ratio R_0. The non-self-similar nature due to the finite radial extent is demonstrated and discussed by plotting the stress and deformation paths of various material points in the $p-q$ and $v-\ln p$ planes, respectively. Finally, the accuracy of existing approximate solutions for the expansion analysis of a thick-walled cylinder of critical state soil is examined. The present solution can serve as a benchmark for numerical simulations and a tool to capture the finite boundary effect during pressuremeter tests in small-sized calibration chambers. It also provides a general framework for many other non-self-similar cavity expansion/contraction problems (e.g. those considering thermo-hydro-mechanical coupling and loading/unloading history).

Declaration of competing interest

The authors declare that they have no known competing financial interests or personal relationships that could have appeared to influence the work reported in this paper.

Acknowledgments

We acknowledge the funding support from the National Key Research and Development Program of China (Grant No. 2023YFB2604004), the National Natural Science Foundation of China (Grant No. 52108374), the "Taishan" Scholar Program of Shandong Province, China (Grant No. tsqn201909016). The first author also thanks the financial support from the China Scholarship Council for his study at the University of Leeds.

List of symbols

a_0, a, a_{end}	initial, current, and final radii of the inner cylinder wall
b_0, b	initial and current radii of the outer cylinder wall
c	cohesion in the Mohr-Coulomb model
$\mathrm{D}(\cdot)$	material time differential of $(\cdot)$ for a material point
$\mathrm{d}(\cdot)$	spatial differential of $(\cdot)$ for a given time
E	elastic modulus
E_0	constant elastic modulus
f, g	yield function and plastic potential
i, j	node number and load step number
M, Γ, λ, κ	critical state parameters
n, r^*	additional material constants in the CASM
p, q	mean effective stress and deviatoric stress
p_0, q_0	initial mean effective stress and deviatoric stress
p_{c0}, p_{c}	initial and current isotropic yield pressures
p_ρ, q_ρ	mean effective stress and deviatoric stress at the elastic-plastic boundary
R_0	initial overconsolidation ratio
r_0, r	initial and current radii of a material point
$r_{(i)}^{(0)}$	initial radius of the i-th node
u	radial displacement of a material point
v_0, v	initial and current specific volumes of soil
$\boldsymbol{x}_{(i)}^{(j)}$	information vector for the i-th node in the j-th load step
ε_k^{e}, ε_k^{p}	elastic component of ε_k $(k = r, \theta, z)$
ε_r, ε_θ, ε_z	total radial, circumferential, and vertical strains
ε_v^{p}, ε_v	plastic and total volumetric strains
η	stress ratio
φ, ψ	friction angle and dilation angle in the Mohr-Coulomb model
μ	Poisson's ratio
ρ_0, ρ	initial and current radii of the elastic-plastic boundary
σ_a	inner cavity pressure
σ_{h}, σ_{v}	initial horizontal and vertical stresses
σ_r, σ_θ, σ_z	effective radial, circumferential, and vertical stresses
$\sigma_{r\rho}$	effective radial stress at the elastic-plastic boundary
χ	auxiliary variable

References

Bigoni, D., Laudiero, F., 1989. The quasi-static finite cavity expansion in a non-standard elasto-plastic medium. Int. J. Mech. Sci. 31 (11–12), 825–837.
Cao, L.F., Teh, C.I., Chang, M.F., 2001. Undrained cavity expansion in modified Cam clay. Geotechnique 51 (4), 323–334.
Carter, J.P., Yu, H.S., 2022. Cavity expansion in cohesive-frictional soils with limited dilation. Geotechnique 73 (7), 629–635.
Chadwick, P., 1959. The quasi-static expansion of a spherical cavity in metals and ideal soils. Q. J. Mech. Appl. Math. 12 (1), 52–71.
Chang, M.F., Teh, C.I., Cao, L.F., 2001. Undrained cavity expansion in modified Cam clay II: application to the interpretation of the piezocone test. Geotechnique 51 (4), 335–350.
Chen, H., Li, L., Li, J., Sun, D., 2020. Elastoplastic solution to drained expansion of a cylindrical cavity in anisotropic critical-state soils. J. Eng. Mech. 146 (5), 04020036.
Chen, H., Mo, P.Q., 2022. An undrained expansion solution of cylindrical cavity in SANICLAY for K0-consolidated clays. J. Rock Mech. Geotech. Eng. 14 (3), 922–935.
Chen, S.L., Abousleiman, Y.N., 2012. Exact undrained elasto-plastic solution for cylindrical cavity expansion in modified Cam Clay soil. Geotechnique 62 (5), 447–456.
Chen, S.L., Abousleiman, Y.N., 2013. Exact drained solution for cylindrical cavity expansion in modified Cam Clay soil. Geotechnique 63 (6), 510–517.
Chen, S.L., Liu, K., 2019. Undrained cylindrical cavity expansion in anisotropic critical state soils. Geotechnique 69 (3), 189–202.
Cheng, Y., Yang, H.W., Sun, D.A., 2018. Cavity expansion in unsaturated soils of finite radial extent. Comput. Geotech. 102, 216–228.
Cheng, Y., Yang, H.W., 2019. Exact solution for drained spherical cavity expansion in saturated soils of finite radial extent. Int. J. Numer. Anal. Methods GeoMech. 43 (8), 1594–1611.
Collins, I.F., Pender, M.J., Wang, Y., 1992. Cavity expansion in sands under drained loading conditions. Int. J. Numer. Anal. Methods GeoMech. 16 (1), 3–23.
Collins, I.F., Yu, H.S., 1996. Undrained cavity expansions in critical state soils. Int. J. Numer. Anal. Methods GeoMech. 20 (7), 489–516.
Fahey, M., 1986. Expansion of a thick cylinder of sand: a laboratory simulation of the pressuremeter test. Geotechnique 36 (3), 397–424.
Ghafghazi, M., Shuttle, D., 2008. Interpretation of sand state from cone penetration resistance. Geotechnique 58 (8), 623–634.
Gibson, R.E., Anderson, W.F., 1961. In-situ measurement of soil properties with pressuremeter. Civ. Eng. Pub. Works Rev. 56 (658), 615–618.
Hill, R., 1950. The Mathematical Theory of Plasticity. Oxford University Press, London, UK.
Hughes, J.M.O., Wroth, C.P., Windle, D., 1977. Pressuremeter tests in sands. Geotechnique 27 (4), 455–477.
Jewell, R.J., Fahey, M., Wroth, C.P., 1980. Laboratory studies of the pressuremeter test in sand. Geotechnique 30 (4), 507–531.
Li, G.Y., Mo, P.Q., Li, C., Hu, J., Zhuang, P.Z., Yu, H.S., 2023. Loading-unloading of spherical and cylindrical cavities in cohesive-frictional materials with arbitrary radially symmetric boundary conditions. Appl. Math. Model. 124, 488–508.
Li, L., Li, J., Sun, D.A., 2016. Anisotropically elasto-plastic solution to undrained cylindrical cavity expansion in K0-consolidated clay. Comput. Geotech. 73, 83–90.
Li, L., Chen, H., Li, J., 2021a. An elastoplastic solution to undrained expansion of a cylindrical cavity in SANICLAY under plane stress condition. Comput. Geotech. 132, 103990.
Li, L., Chen, H., Li, J., 2021b. An elastoplastic solution for cylindrical cavity expansion under constant water content conditions in anisotropic unsaturated soils. Comput. Geotech. 139, 104323.
Mair, R.J., Taylor, R.N., 1993. Prediction of clay behaviour around tunnels using plasticity solutions. In: Predictive Soil Mechanics: Proceedings of the Wroth Memorial Symposium. Thomas Telford, Oxford, UK, pp. 449–463.
Mo, P.Q., Yu, H.S., 2018. Drained cavity expansion analysis with a unified state parameter model for clay and sand. Can. Geotech. J. 55 (7), 1029–1040.
Mo, P.Q., Gao, X.W., Yang, W., Yu, H.S., 2020. A cavity expansion–based solution for interpretation of CPTu data in soils under partially drained conditions. Int. J. Numer. Anal. Methods GeoMech. 44 (7), 1053–1076.
Mo, P.Q., Chen, H., Yu, H.S., 2022. Undrained cavity expansion in anisotropic soils with isotropic and frictional destructuration. Acta Geotech 17 (6), 2325–2346.
Osinov, V.A., Cudmani, R., 2001. Theoretical investigation of the cavity expansion problem based on a hypoplasticity model. Int. J. Numer. Anal. Methods GeoMech. 25 (5), 473–495.
Pournaghiazar, M., Russell, A.R., Khalili, N., 2013. Drained cavity expansions in soils of finite radial extent subjected to two boundary conditions. Int. J. Numer. Anal. Methods GeoMech. 37 (4), 331–352.
Randolph, M.F., Dolwin, R., Beck, R., 1994. Design of driven piles in sand. Geotechnique 44 (3), 427–448.
Russell, A.R., Khalili, N., 2006. On the problem of cavity expansion in unsaturated soils. Comput. Mech. 37 (4), 311–330.
Salgado, R., Mitchell, J.K., Jamiolkowski, M., 1997. Cavity expansion and penetration resistance in sand. J. Geotech. Geoenviron. Eng. 123 (4), 344–354.
Schnaid, F., Houlsby, G.T., 1991. An assessment of chamber size effects in the calibration of in situ tests in sand. Geotechnique 41 (3), 437–445.
Silvestri, V., Abou-Samra, G., 2012. Analytical solution for undrained plane strain expansion of a cylindrical cavity in modified cam clay. Geomech. Eng. 4 (1), 19–37.
Song, X.G., Yang, H., Yue, H.Y., Guo, X., Yu, H.S., Zhuang, P.-Z., 2022. Closed-form solutions for large strain analysis of cavity contraction in a bounded Mohr-Coulomb medium. Eur. J. Environ. Civ. Eng. 26 (10), 4548–4575.
Su, D., 2021. Drained solution for cylindrical cavity expansion in modified Cam Clay soil under constant vertical stress. Can. Geotech. J. 58 (2), 176–189.
Vesic, A.S., 1972. Expansion of cavities in infinite soil mass. J. Soil Mech. Found Div. 98 (SM3), 265–290.

Vrakas, A., 2016. A rigorous semi-analytical solution for undrained cylindrical cavity expansion in critical state soils. Int. J. Numer. Anal. Methods GeoMech. 40 (15), 2137–2160.
Wang, X., Chen, S., 2022. Revisiting undrained cavity expansion problem in critical state soils: a simple graph-based approach. Int. J. Numer. Anal. Methods GeoMech. 46 (12), 2356–2374.
Yang, C., Li, J., Li, L., Sun, D.A., 2021. Expansion responses of a cylindrical cavity in overconsolidated unsaturated soils: a semi-analytical elastoplastic solution. Comput. Geotech. 130, 103922.
Yang, H., Yu, H.S., Chen, X., Zhuang, P.-Z., 2023. Rigorous solution for drained analysis of spherical cavity expansion in soils of finite radial extent. Comput. Geotech. 160, 105516.
Yu, H.S., Houlsby, G.T., 1991. Finite cavity expansion in dilatant soils: loading analysis. Geotechnique 41 (2), 173–183.
Yu, H.S., 1992. Expansion of a thick cylinder of soils. Comput. Geotech. 14 (1), 21–41.
Yu, H.S., 1993. Finite elastoplastic deformation of an internally pressurized hollow sphere. Acta Mech. Solida Sin. 6 (1), 81–97.
Yu, H.S., 1998. CASM: a unified state parameter model for clay and sand. Int. J. Numer. Anal. Methods GeoMech. 22 (8), 621–653.
Yu, H.S., Rowe, R.K., 1999. Plasticity solutions for soil behaviour around contracting cavities and tunnels. Int. J. Numer. Anal. Methods GeoMech. 23 (12), 1245–1279.
Yu, H.S., 2000. Cavity Expansion Methods in Geomechanics. Kluwer Academic Publishers, Dordrecht, The Netherlands.
Yu, H.S., Carter, J.P., 2002. Rigorous similarity solutions for cavity expansion in cohesive-frictional soils. Int. J. GeoMech. 2 (2), 233–258.
Zhou, H., Kong, G., Liu, H., Laloui, L., 2018. Similarity solution for cavity expansion in thermoplastic soil. Int. J. Numer. Anal. Methods GeoMech. 42 (2), 274–294.
Zhou, H., Liu, H., Wang, Z., Ding, X., 2021. A unified and rigorous solution for quasi-static cylindrical cavity expansion in plasticity constitutive models. Comput. Geotech. 135, 104162.
Zhuang, P.Z., Yu, H.S., 2018. Uplift resistance of horizontal strip anchors in sand: a cavity expansion approach. Géotech. Lett. 8 (4), 284–289.
Zhuang, P.Z., Yu, H.S., Mooney, S.J., Mo, P.Q., 2021a. Loading and unloading of a thick-walled cylinder of critical-state soils: large strain analysis with applications. Acta Geotech 16, 237–261.
Zhuang, P.Z., Yue, H.Y., Song, X.G., Yang, H., Yu, H.S., 2021b. Uplift behavior of pipes and strip plate anchors in sand. J. Geotech. Geoenviron. Eng. 147 (11), 04021126.
Zhuang, P.Z., Yang, H., Yue, H.Y., Fuentes, R., Yu, H.S., 2022. Plasticity solutions for ground deformation prediction of shallow tunnels in undrained clay. Tunn. Undergr. Space Technol. 120, 104277.

He Yang is a PhD Candidate of Civil Engineering, at School of Civil Engineering, University of Leeds. He obtained his BEng degree in Civil Engineering from Shandong University, China in 2018, and MEng degree in Highway and Railway Engineering from Shandong University, China, in 2021. His research interests include (1) Cavity expansion theory and applications; (2) Intepretation of in-situ tests; (3) Constitutive modelling of unsaturated soils; and (4) Soil-structure interations in piles, pipelines, plate anchors, and tunnels. He has published over 10 papers on peer-review journals.